Supplemental Material: Soft Pneumatic Actuator Design using Differentiable Simulation

Arvi Gjoka
New York University / Courant
New York, USA
arvi.gjoka@nyu.edu

Espen Knoop
Disney Research
Zurich, Switzerland
espen.knoop@disneyresearch.com

Moritz Bächer
Disney Research
Zurich, Switzerland
moritz.baecher@disneyresearch.com

Denis Zorin
New York University / Courant
New York, USA
dzorin@cs.nyu.edu

Daniele Panozzo
New York University / Courant
New York, USA
panozzo@nyu.edu

ACM Reference Format:
Arvi Gjoka, Espen Knoop, Moritz Bächer, Denis Zorin, and Daniele Panozzo. 2024. Supplemental Material: Soft Pneumatic Actuator Design using Differentiable Simulation. In *Special Interest Group on Computer Graphics and Interactive Techniques Conference Conference Papers '24 (SIGGRAPH Conference Papers '24), July 27-August 1, 2024, Denver, CO, USA.* ACM, New York, NY, USA, 6 pages. https://doi.org/10.1145/3641519.3657467

1 DERIVATION OF GRADIENT AND HESSIAN OF E_p

The volume can be expressed as a surface integral over the boundary of $\Omega_C(x+u)$ via the divergence theorem

$$E_p(x,u) = P \oint_{\partial\Omega_C(x+u)} s \cdot \hat{n}(s)\, ds \tag{1}$$

where $\hat{n}(s)$ is the solution-dependent normal of the deformed surface. We can make change of variables modification to express this as an integral over the rest surface.

$$E_p(x,u) = P \oint_{\partial\Omega_C(x)} s \cdot g_3(s+u(s))\, ds \tag{2}$$

where $g_3 = g_1 \times g_2$, with $g_1 = \frac{\partial x}{\partial \xi}$, $g_2 = \frac{\partial x}{\partial \eta}$ and ξ, η parametrize the reference surface element.

It then stands that

$$\hat{n} = \frac{g_3}{||g_3||} = \frac{g^1 \times g^2}{||g^1 \times g^2||} \tag{3}$$

The gradient of the energy is then

$$\nabla E_p(x,u)[\phi_i] = P \oint_{\partial\Omega_C(x)} \phi_i \cdot g_3(x+u)\, dx \tag{4}$$

and the hessian

$$\Delta E_p(x)[\phi_i,\phi_j] = P \sum_{\alpha=1,2} \oint_{\partial\Omega_C(x)} (g_3 \wedge g^\alpha)^T \phi_j \cdot \frac{\partial \phi_i}{\partial x} + \left((g_3 \wedge g^\alpha)\frac{\partial \phi_j}{\partial x}\right) \cdot \phi_i\, dx \tag{5}$$

where g^α are dual vectors to g_α.

2 MATERIAL CHARACTERIZATION

In order to effectively optimize the design of an object under inflation, we need to have an accurate material model that fits a material's behavior under various settings. We take inspiration from the material characterization work of [Schumacher et al. 2020] and decide to use a 3 parameter Mooney Rivlin model, which is given by

$$\Psi_{MR} = C_{10}(\bar{I}_1 - 3) + C_{01}(\bar{I}_2 - 3) + C_{11}(\bar{I}_1 - 3)(\bar{I}_2 - 3) + D_1(J-1)^2 \tag{6}$$

Since we're anticipating large deformations of pneumatic actuators, we make a modification to the volume preservation term of the material model, replacing $(J-1)^2$ by $(\ln J)^2$. This should prevent elements from inverting in the large strain cases. The energy density function then becomes

$$\Psi_{MR} = C_{10}(\bar{I}_1 - 3) + C_{01}(\bar{I}_2 - 3) + C_{11}(\bar{I}_1 - 3)(\bar{I}_2 - 3) + D_1(\ln J)^2 \tag{7}$$

We also draw inspiration from the parameter fitting model outlined in the aforementioned work. Instead of fitting material parameters on a multitude of uniaxial compression, extension and shear tests, we instead perform uniaxial compression and extension of specimens bonded (and thereby fixed) on both ends. This produces a multitude of strain values throughout the specimen, densely sampling the material behavior along the stress-strain curve for purposes of material parameter fitting.

We use this technique to come up with material parameters matching uniaxial compression and extension tests. The material we use is Smooth-On Mold Max 14NV, for which the inferred parameters are $C_{10} = 55000,\ C_{01} = 5000,\ C_{11} = 1700,\ D_1 = 1000000$.

For new material physics, such as Mooney Rivlin model, we need to compute a few terms to support differentiability. Firstly,

SIGGRAPH Conference Papers '24, July 27-August 1, 2024, Denver, CO, USA

ACM ISBN 979-8-4007-0525-0/24/07…$15.00
https://doi.org/10.1145/3641519.3657467

$\frac{\partial G}{\partial u}$ needs to be computed for the adjoint solve in Eq. 5 of Sec. 3 in the main text. However, this quantity is also needed for the hessian matrix of the forward simulation so no extra derivations are needed. What we do need to compute is $\frac{\partial G}{\partial q}$, or the sensitivity of the material model with respect to the differentiation parameters, e.g. shape in this case.

3 CLOSED CHAMBER COMPRESSION TEST

We design an experiment to validate $E_p(x,u)$ on a closed chamber with a fixed amount of air by designing a closed cavity, compressing it with a column testing machine, and observing the deformation. We also measure the force exerted by the object for varying compression levels and compare this with simulation. For a closed cavity in silicone, we model the compression as an adiabatic process. The pressure value during the compression is given by

$$P = P_0 \frac{V_0^\gamma}{V^\gamma}, \tag{8}$$

which we can substitute into the expression for $E_p(x,u)$ from Eq. 6 in Section 4.1 of the main text

$$W = \int_{V_0}^{V(x+u)} P_0 \frac{V_0^\gamma}{V(x,u)^\gamma} dV, \tag{9}$$

which can be integrated analytically to produce an expression for $E_p(x,u)$ in the adiabatic case

$$E_p(x,u) = \frac{P_0 V_0^\gamma}{1-\gamma} \left(\oint_{\partial\Omega_C(x+u)} s \cdot \hat{n}(s)\, ds \right)^{1-\gamma}. \tag{10}$$

The gradient of the energy remains the same as Eq. 4, except the pressure is computed according to Eq. 8 as a function of the chamber volume:

$$\nabla E_p(x,u)[\phi_i] = \frac{P_0 V_0^\gamma}{V(x,u)^\gamma} \oint_{\partial\Omega_C(x)} \phi_i \cdot g_3(x+u)\, dx. \tag{11}$$

Since the pressure is now shape-dependent, we need a modification to the hessian to account for this, which becomes:

$$\begin{aligned} \Delta E_p(x)[\phi_i,\phi_j] = \frac{P_0 V_0^\gamma}{V(x,u)^\gamma} \sum_{\alpha=1,2} \oint_{\partial\Omega_C(x)} & (g_3 \wedge g^\alpha)^T \phi_j \cdot \frac{\partial \phi_i}{\partial x} \\ & + \left((g_3 \wedge g^\alpha) \frac{\partial \phi_j}{\partial x} \right) \cdot \phi_i \, dx \\ - \frac{\gamma P_0 V_0^\gamma}{V(x,u)^{\gamma-1}} & \left(\oint_{\partial\Omega_C(x)} \phi_i \cdot g_3(x+u)\, dx \right) \\ & \cdot \left(\oint_{\partial\Omega_C(x)} \phi_j \cdot g_3(x+u)\, dx \right), \end{aligned} \tag{12}$$

where the last term accounts for the dependence of pressure on the solution u. This is noteworthy because as opposed to the isobaric (constant pressure) case above, adiabatic processes lead to block-dense hessians as the displacement of any vertex i on the chamber surface will lead to a change in force, $\nabla E_p(x,u)[\phi_j]$, at any other node j on the closed surface. Niewiarowski et al. [2020] outlines a method for reducing the resulting dense linear solve in the Newton optimization into a sparse linear solve with extra algebraic operations using the Sherman–Morrison formula.

Whereas the qualitative comparison is given in the main text, we plot the force-displacement graphs from the column testing machine and the simulation in Fig 1. We observe that the general characteristics of the predicted and experimental data plots are similar, albeit with a roughly 20% difference in magnitude. We believe this disparity is due to the epoxy glue used to join the two silicone halves of the chambers, which changed the geometry slightly and has material properties different from the silicone.

4 PHYSICAL EXPERIMENTS

For completeness, we show the rest and inflated states of the physical experiments in Figs. 2-4 below

REFERENCES

Alexander Niewiarowski, Sigrid Adriaenssens, and Ruy Marcelo Pauletti. 2020. Adjoint optimization of pressurized membrane structures using automatic differentiation tools. *Computer Methods in Applied Mechanics and Engineering* 372 (2020), 113393. https://doi.org/10.1016/j.cma.2020.113393

Christian Schumacher, Espen Knoop, and Moritz Bächer. 2020. Simulation-Ready Characterization of Soft Robotic Materials. *IEEE Robotics and Automation Letters* 5, 3 (2020), 3775–3782.

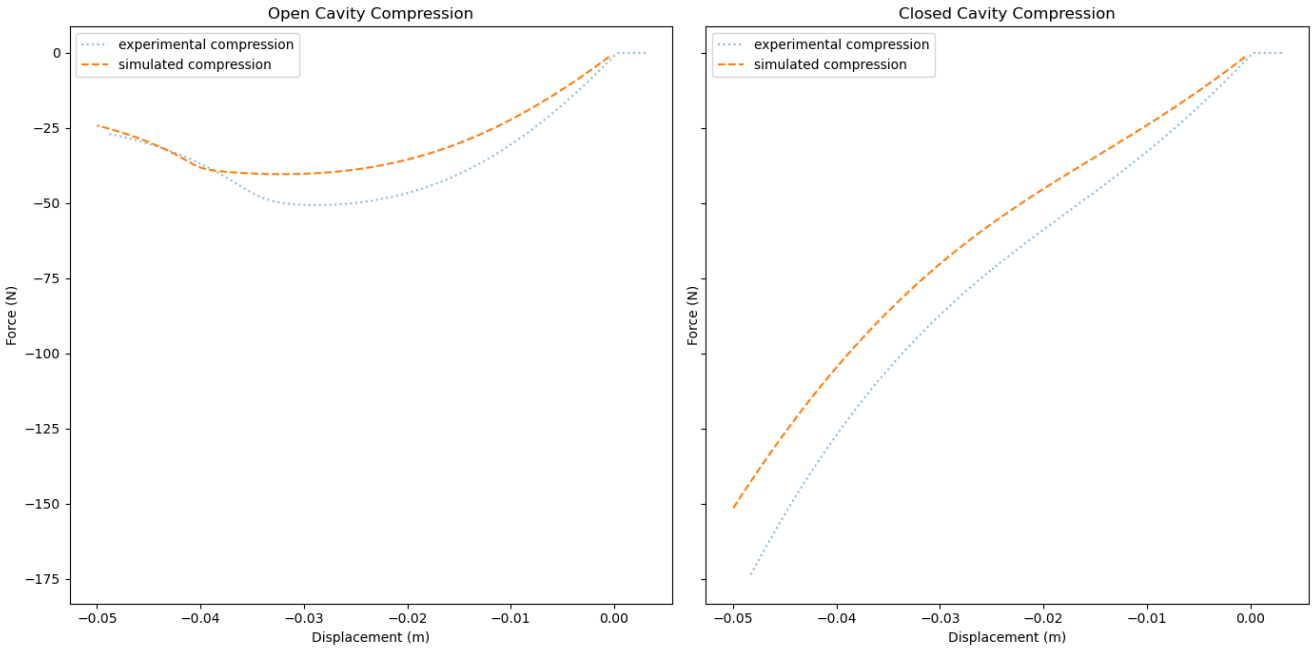

Figure 1: Quantitative comparison of open and closed cavity compression.

(a) Rest pose

(b) Inflated pose

Figure 2: Inflation of a frog.

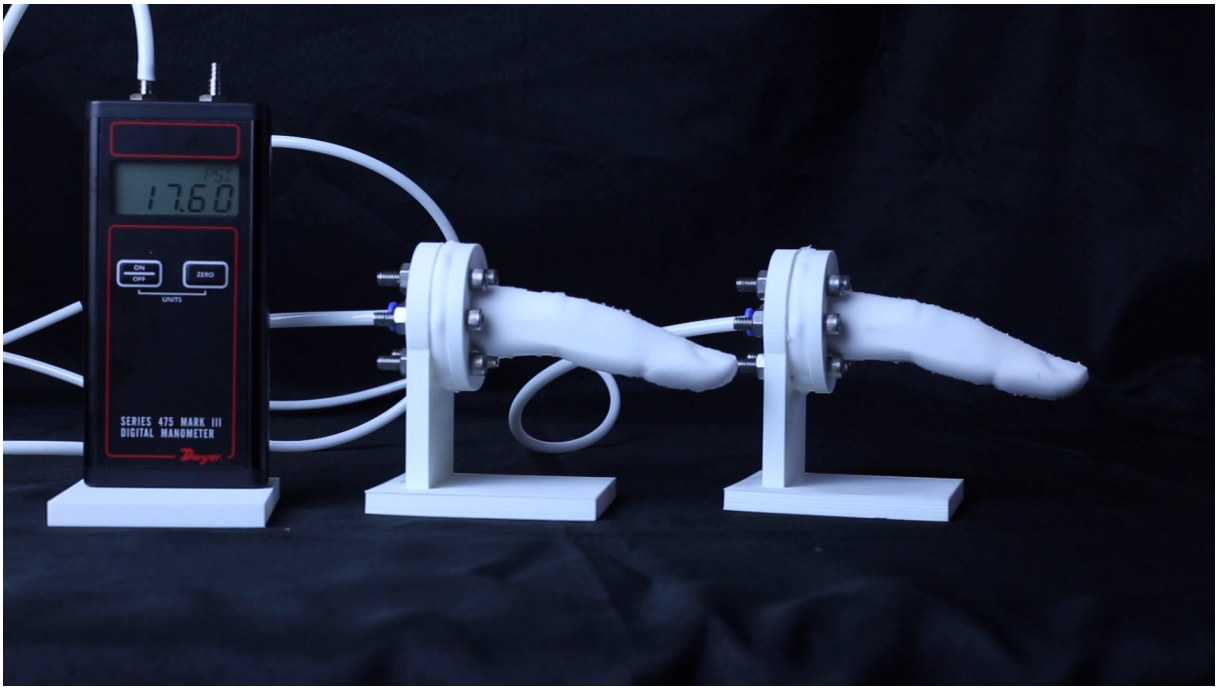

(a) Rest pose

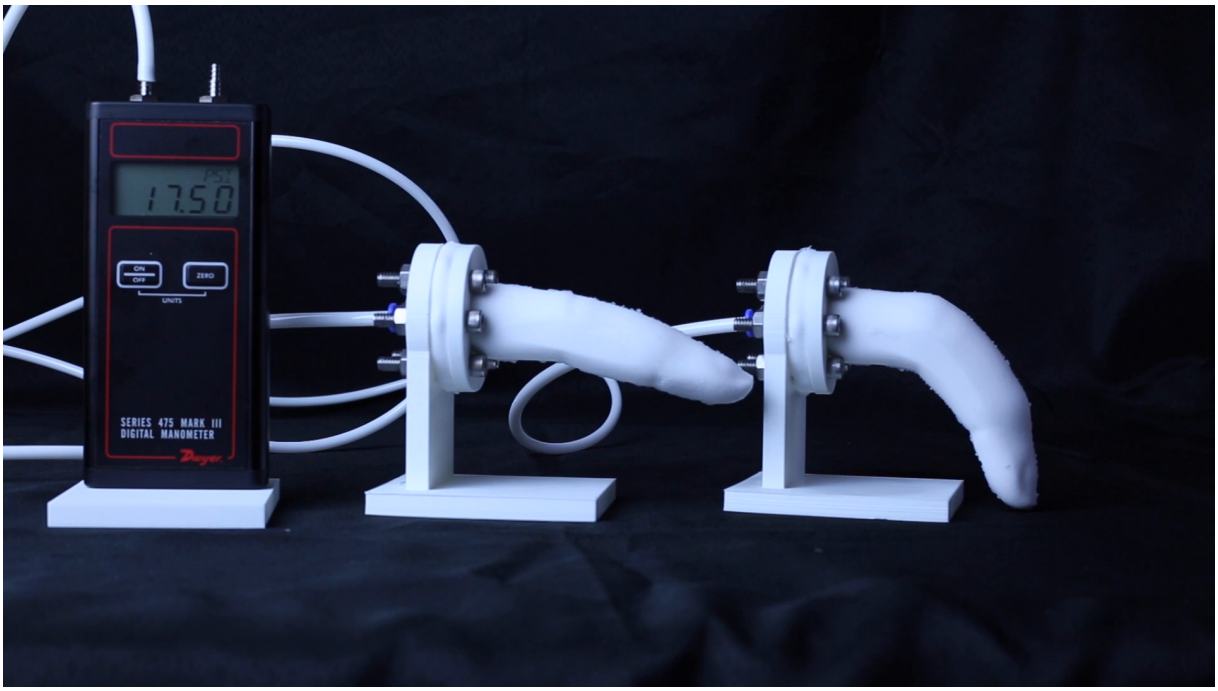

(b) Inflated pose

Figure 3: Inflation of a finger.

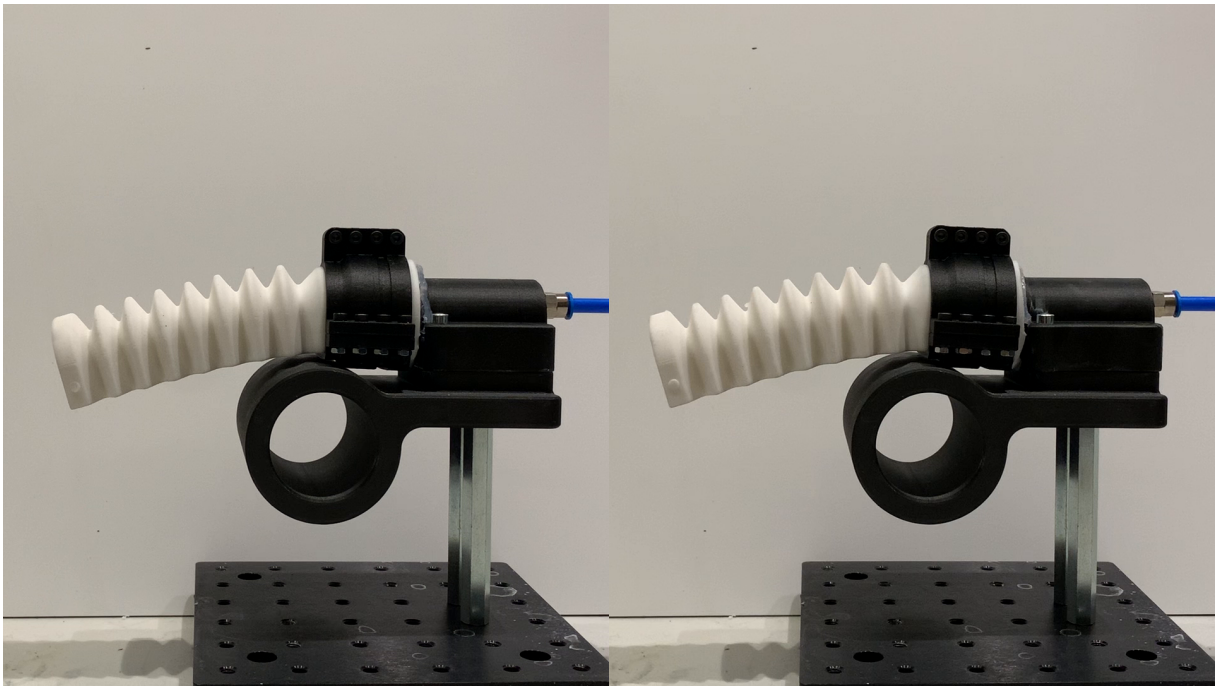

(a) Rest pose

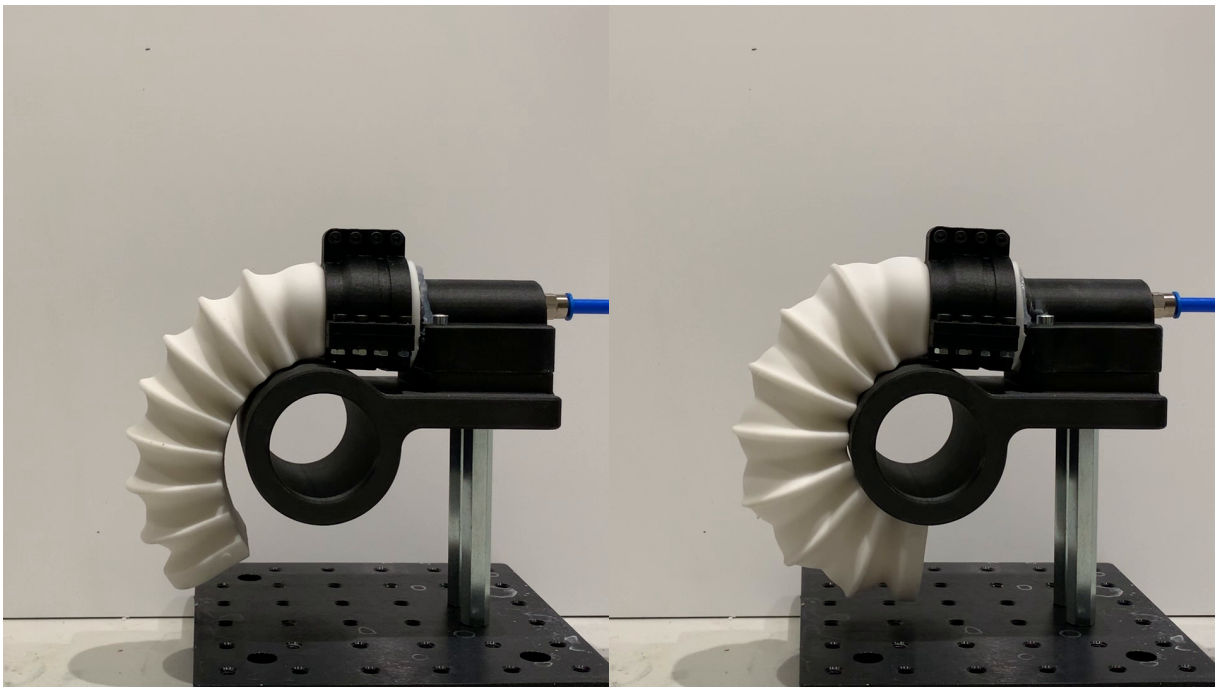

(b) Inflated pose

Figure 4: Inflation of a gripper.